The N-terminal domain of tumor suppressor p53 is involved in the molecular interaction with the anti-apoptotic protein Bcl-Xl

Huibin Xu, Jeff Tai, Hong Ye, Cong Bao Kang, Ho Sup Yoon *

Division of Structural and Computational Biology, School of Biological Sciences, Nanyang Technological University, 60 Nanyang Drive, Singapore 637511, Singapore

** Corresponding author. Fax: +65 6791 3856*

E-mail address: hsyoon@ntu.edu.sg (H.S. Yoon)

Abstract

Emerging evidences suggest that transcription-independent mechanism of p53 appears to make an important contribution to the overall p53-dependent apoptosis. Recently, it has been postulated that the DNA-binding domain of p53 can interact with Bcl-Xl, and subsequently the proposed molecular interaction has been shown by NMR studies. Interestingly, Chipuk et al. [Cancer Cell 4 (2003) 371] reported that the N-terminal domain of p53 (p53NTD) alone is necessary and sufficient to induce transcription-independent apoptosis. To further define and understand the nature of the molecular recognition between p53 and Bcl-Xl, our current study focuses on p53NTD. We first demonstrated the molecular interaction between p53NTD and Bcl-Xl by co-expressing and purifying the complex. Second, to define the binding interface of the molecular interaction, which is not previously characterized, in the current we employed a NMR-based binding study, showing that the

binding site on Bcl-Xl is located in the region including α4, the N- and C-termini of α3, the N-terminus of α5, and the central part of α2. To further probe this observation, we then performed fluorescence resonance energy transfer (FRET) assay in cells. The FRET efficiency detected between the donor and acceptor molecules appears to suggest the presence of molecular interaction of p53NTD with Bcl-Xl in cells. Taken together, our data suggest that p53NTD interacts with Bcl-Xl but the characteristic of the molecular interaction appears to be different from that of the DNA-binding domain of p53.

Keywords: p53; p53NTD; Bcl-Xl; NMR; Apoptosis; FRET

---

p53 is one of most important tumor suppressor proteins [1]. The loss of p53 function has been associated with human cancers, indicating that p53 plays a key role in the anti-cancer pathway [2]. p53 is a transcriptional factor and exerts most of its tumor suppressor activities as a transcriptional factor on the regulation of cell cycle arrest, senescence, differentiation, and apoptosis [3–5]. While transcription-dependent mechanism of p53 on the induction of apoptosis has been well established, recent evidences demonstrated that the p53-dependent apoptosis is also observed in a transcription-independent manner [6–9]; In cell-free models, p53 can induce caspase-3 activity or cytochrome *c* release [10,11]. It has been shown that p53, in response to oncogenic stress inducers, can localize to the mitochondria and induce apoptotic cell death, without exerting a transcriptional activity [12–14].

Bcl-2 family proteins are central in the mitochondria-mediated apoptosis [15]. It has been shown that p53 can directly bind Bcl-2 and Bcl-Xl, and consequently inhibit their anti-apoptotic activities [16], suggesting that the function of cytoplasmic p53 is

transcription-independent. Recently, it has been postulated by molecular modeling that the DNA-binding domain of p53 could interact with Bcl-Xl [16], and subsequently, its molecular interaction with Bcl-Xl was shown through a NMR-binding study [17]. However, interestingly, the results from Chipuk et al. [18] demonstrated that the amino terminus of p53 (p53NTD) spanning M1-T102 is necessary and sufficient to induce transcription-independent apoptosis. The p53NTD contains the transcription activation domain (TAD) and a proline-rich region [19,20]. The TAD works as a transcription factor to regulate specific gene expression [19]. The Mdm2-binding site is located in this domain [21,22]. The proline-rich domain was shown to contribute to its apoptosis activity [20]. The flexible and disordered nature of this domain also has been reported [23,24]. Apparently, the N-terminal domain of the tumor suppressor p53 exerts a dynamic regulatory mechanism and the binding characteristics observed between p53 and other regulatory molecules including the anti-apoptotic molecule Bcl-Xl remain to be further understood. Thus, in our study, to better define the role of the cytoplasmic p53 and further understand transcription-independent mechanism of p53, here we focused on the study on p53NTD and investigated its molecular interaction with Bcl-Xl.

Materials and methods

Materials. Antibodies against Bcl-Xl (S-18) and p53 (FL-393) were purchased from Santa Cruz Biotech (Santa Cruz, CA, USA). Ni^{2+}–NTA resin was from Qiagen (Hilden, Germany). Isopropyl-thio-β-D-galactopyranoside (IPTG) was from Promega (Madison, WI, USA). HiPrep 26/ 60 gel Sephacryl S-200 gel filtration column was from Amersham Biosciences (Buckinghamshire, UK). Cell lines were from American Type Culture Collection (ATCC) (Manassas, VA). RPMI medium 1640 was from Invitrogen (Carlsbad, CA). ^{15}N-

NH_4Cl was from Cambridge Isotope Laboratories (MA, USA). All the other chemicals were obtained from Sigma (St. Louis, MO).

Protein expression and purification. Bcl-Xl lacking the transmembrane domain (Bcl-XlΔTM) and uniformly ^{15}N-labeled Bcl-XlΔTMΔ(M45- A84), in which the residues from M45 to A84 were deleted, expressed, and purified using the protocol as previously described [25]. p53NTD (1–102) was amplified from pBabePuro.p53ERTAM plasmid (a gift from Professor Gerald I. Evan, U. of California San Francisco, USA) by polymerase chain reaction and inserted into pET-16b expression plasmid (Novagen) to generate pET16b-p53NTD plasmid. p53NTD was expressed either on LB media or M9 media containing $^{15}NH_4Cl$ (for uniformly ^{15}N-labeled p53NTD). After the A_{600} reached 0.8, the protein was induced by IPTG for 3 h at 25 °C. Then, proteins were purified using Ni^{2+}–NTA affinity column and Sephacryl S-200 gel filtration column chromatography. All the proteins were stored at 4 °C before use.

Tissue culture and transfection. NCI-H1299, p53-deficient cells, were cultured at 37 °C under 10% CO_2 in RPMI1640 supplemented with 10% FBS, 100 μg/ml penicillin–streptomycin (Invitrogen). Transfections of 1 μg of the appropriate plasmids into log-phase growth NCI-H1299 cells were carried out using Lipofectamine 2000 reagents according to the manufacturer's protocol (Invitrogen). Overnight cell cultures were then fixed in 3.7% paraformaldehyde for 20 min and mounted on slides. Slowfade antifade kit was used as a mounting solution (Molecular Probes).

NMR-binding assay. All NMR data were acquired at 298 K on either a Bruker Avance AV700 or Avance AV600 spectrometer, equipped with a cryoprobe accessory. Uniformly ^{15}N-labeled Bcl-XlΔ TMΔ(M45-A84) sample contained 0.5 mM protein in 90% H_2O/10% D_2O in 20 mM phosphate, pH 6.5, 50 mM NaCl, 1 mM DTT, and 0.01%

NaN_3. Chemical shift perturbations to Bcl-Xl were monitored with ^{15}N-heteronuclear single quantum correlation spectroscopy (HSQC) upon the addition of different amounts of p53NTD. Uniformly ^{15}N-labeled p53NTD sample contained 0.25 mM protein in the same buffer. Chemical shift perturbations to p53NTD were monitored with ^{15}N HSQC upon addition of 0.375 mM Bcl-Xl. NMR data were processed and analyzed on Linux workstations using Bruker Topspin software and NMRview5.2 [26].

Western blotting. Proteins were separated on 12% SDS–PAGE and transferred to polyvinylidene difluoride (PVDF) membrane. The PVDF membrane was first blocked with 5% milk in TBS buffer (20 mM Tris–HCl, pH 8.0, 150 mM NaCl) and then incubated with primary antibody in TBS buffer containing 0.2% milk for 2 h at 37 °C. The immunoreactivity was detected using Immune-Star Chemiluminescent protein detection system (Bio-Rad Laboratories).

Co-expression of p53NTD and Bcl-Xl in Escherichia coli. Bcl-Xl and p53NTD were constructed into the dual promoter plasmid pETDuet (Novagen). The pETDuet-p53NTD/Bcl-X plasmid was transformed into *E. coli* BL21(DE3). The proteins were induced and purified as described [27]. The protein fractions were then analyzed by SDS–PAGE followed by Western blot.

Fluorescence resonance energy transfer assay. A Zeiss LSM510 META confocal microscope was employed for fluorescence resonance energy transfer (FRET) analysis using the acceptor photobleaching method as described [28,29] with minor modifications. Five images were collected consecutively at 0.15% of the laser intensity in CFP and YFP channels before and after bleaching of YFP by scanning 150 times at 75% laser intensity. An unbleached cell in the same field was used as a background control to determine CFP

fluctuations during FRET analysis. Fluorescence intensity was measured in the region where p53NTD and Bcl-Xl co-localized. FRET efficiency was calculated as $E_F = (I_6 - I_5) \times 100/I_6$ [29]. I_5 and I_6 represent the CFP fluorescence intensities of the fifth and sixth images immediately before and after photobleaching of YFP. The experiment was repeated three times and each set of FRET or control experiments consists of at least 10 cells. The FRET efficiency is presented as the mean percentage of increase in fluorescence intensity with standard deviation.

Results

Expression and purification the N-terminal domain of p53

p53 contains three functional domains: the N-terminal domain in which the TAD and proline-rich domains are located, the central DNA-binding domain, and the C-terminal oligomerization domain (Fig. 1A). In the current study, p53NTD (1–102) was expressed in *E. coli* cells and purified by Ni^{2+}–NTA affinity column and subsequently further purified by Sephacryl S-200 gel filtration column chromatography. As shown in Fig. 1B, we were able to purify p53NTD to near homogeneity after the gel filtration. The purified p53NTD was confirmed by Western blot analysis (Fig. 1B, lane 7). The calculated molecular weight of p53NTD is about 14 kDa, however, on a SDS–PAGE gel, it migrates around at 21 kDa, suggesting that the domain might not be structurally rigid. We then performed 2D NMR ^{1}H–^{15}N single quantum correlation spectroscopy (HSQC) to monitor the amide ^{1}H and ^{15}N chemical shifts of uniformly ^{15}N-labeled p53NTD. Our data show that the amide proton chemical shifts are poorly resolved, indicating that the purified p53NTD is disordered (Fig. 1C). Taken together, our data suggest that p53NTD

produced in *E. coli* cells is structurally flexible and intrinsically disordered. Our results are consistent with previous observations which showed the disordered nature of p53NTD [24].

p53NTD forms a complex with Bcl-Xl

To probe specific molecular interaction between p53NTD and Bcl-Xl, the two proteins were co-expressed in *E. coli* BL21 (DE3) cells, purified by Ni^{2+}–NTA affinity resin (Fig. 2A), and confirmed by Western blot using anti-p53 and anti-Bcl-Xl antibodies (Fig. 2B). Since p53NTD contains the N-terminal His-tag, while Bcl-Xl has no his-tag, Bcl-Xl can only be purified on a Ni^{2+}– NTA affinity resin through the complex formation with p53NTD. The Western blot results confirmed that the two eluted bands as indicated by the arrows from the affinity column were p53NTD and Bcl-Xl, respectively (Fig. 2B). Our data suggest that p53NTD interacts with Bcl-Xl when they are co-expressed in bacterial cells.

Identification of molecular interaction between p53NTD and Bcl-Xl by a NMR-based binding assay

Identification of the interaction between p53NTD and Bcl-Xl using the co-expression approach prompted us to further check their physical interaction in vitro. Here, we employed a NMR-based binding study using uniformly ^{15}N-labeled Bcl-Xl. The perturbations of chemical shifts in 2D ^{1}H–^{15}N HSQC experiments were monitored before and after the addition of p53NTD. Our NMR results demonstrate that overall the spectrum of 2D ^{1}H–^{15}N HSQC upon the addition of p53NTD remains nearly unchanged except a few residues, indicating that no major conformational change in Bcl-Xl is induced (Fig. 3A). A section

of ^{15}N HSQC spectrum of Bcl-Xl demonstrating its binding is shown enlarged (Fig. 3B). The enlarged section shows that the chemical shifts of L112 and E129 are specifically perturbed in the presence of p53NTD. Additional residues showing the chemical shift perturbations are summarized in Fig. 4A. The residues affected are located in the region including α4, the N- and C-termini of α3, the N-terminus of α5, and the central part of α2. While the majority of the perturbed residues are not located in the hydrophobic groove formed by BH1, BH2, and BH3 regions, L90 and G94 from BH3 region and L112 from α3 are seen to be localized in the groove (Figs. 4A and B). In addition, the molecular interaction between p53NTD and Bcl-Xl was also studied by adding Bcl-Xl to a uniformly ^{15}N-labeled p53NTD and subsequently monitoring the chemical shift changes in a 2D ^{1}H–^{15}N HSQC spectrum (Fig. 5). Our results demonstrate that changes and reductions in chemical shifts were observed upon the addition of Bcl-Xl, suggesting the specific molecular interaction between p53NTD and Bcl-Xl. Since no chemical shift assignments on p53NTD are available, we were not able to identify the residues in p53NTD which participate in the binding with Bcl-Xl.

Molecular interaction between p53NTD and Bcl-Xl is validated by fluorescence resonance energy transfer

To further confirm the molecular interaction between p53NTD and Bcl-Xl, fluorescence resonance energy transfer (FRET) assay was performed in NCI-H1299 cells. For the detection of FRET between the proteins, here, we used yellow fluorescent protein (YFP)-fused p53 (YFP-p53NTD) as acceptor molecule and cyan fluorescent protein (CFP)-fused Bcl-Xl (CFP-Bcl-Xl) as donor molecule. The amount of FRET was calculated as a percentage increase in the donor (CFP) fluorescence intensity after photobleaching the

acceptor (YFP) in a small part of the cell as seen in Fig. 6A. When the YFP acceptor fluorophore was at least 85% selectively bleached, an increase in fluorescence signal in the donor CFP in the region of interest was observed, indicating the occurrence of FRET. The increase in CFP fluorescence intensity in the bleached region (Fig. 6A, black dashed box) was compared to the CFP fluctuation in the unbleached (control) region (Fig. 6A, white dashed box). From the data, the FRET efficiency for the bleached and unbleached samples was 5.11% and 0.54%, respectively (Fig. 6B). Taken together, our FRET data suggest that the FRET is seen between the donor CFP-Bcl-Xl and acceptor YFP-p53NTD, and this appears to be attributed to the molecular interaction between p53NTD and Bcl-Xl in NCI-H1299 cells.

Discussion

Transcription-dependent regulatory mechanism of tumor suppressor p53 has been extensively studied and well defined. However, the biological significance and mechanism of transcription-independent regulation of p53 are less well understood. Previously, it was shown that the cytoplasmic p53 can directly interact with Bcl-Xl at the mitochondrial membrane and induce apoptosis [16]. The DNA-binding domain and Bcl-Xl binding have been proposed by molecular modeling and subsequently its binding interface was checked by NMR studies [16,17]. Interestingly, it has been also demonstrated that the N-terminal domain of p53 (p53NTD) including transactivation domain and proline-rich region is necessary and sufficient for the induction of p53-mediated apoptosis [18]. In this study, we focused our study on the molecular interaction between the N-terminal domain of p53 and Bcl-Xl. p53NTD is shown to be structurally disordered in its native state [24]. p53NTD appears to play an important role in the p53-mediated apoptotic regulation; the regulation

by MDM2 binding and subsequent degradation is well defined [21,22] and the regulation by phosphorylation in p53NTD was also demonstrated [30], and the proline-rich region was shown to bind to SH3 domain [31]. In our study, we expressed p53NTD (1–102) in *E. coli* cells and purified it for biochemical and structural analysis. The p53NTD appears to be stable during and after purification, and from our co-expression study we demonstrated that the p53NTD binds to Bcl-Xl. Our NMR-based binding study led to define the binding interface between p53NTD (1–102) and Bcl-Xl. From our 2D ^{1}H–^{15}N HSQC experiments of ^{15}N-labeled Bcl-Xl, the mapping of the perturbed residues on Bcl-Xl shows that the affected residues are located in the region including $\alpha 4$, the N- and C-termini of $\alpha 3$, the N-terminus of $\alpha 5$, and the central part of $\alpha 2$. Our results indicate that the majority of the affected residues are not localized in the hydrophobic pocket contributed by BH1, BH2, and BH3 regions. A few residues including L90 and G94 from BH3 region and L112 from $\alpha 3$ are noticed to be localized in the hydrophobic groove (Fig. 4). Previously it was shown that the DNA-binding domain of p53 interacts with Bcl-Xl [16]. In that study, the p53-binding site on Bcl-Xl appears to consist of the C-terminus of $\alpha 1$, the loop between $\alpha 3$ and $\alpha 4$, and the loop between $\alpha 5$ and $\alpha 6$. Based upon these observations, the molecular basis for the interaction between the p53NTD and Bcl-Xl appears to be different from that between the DNA-binding domain of p53 and Bcl-Xl. We also investigated the Bcl-Xl-binding site on p53NTD(1–102) by adding Bcl-Xl to a uniformly ^{15}N-labeled p53NTD and subsequently monitoring the chemical shift changes in a 2D ^{1}H–^{15}N HSQC spectrum (Fig. 5). The perturbations in the chemical shifts of ^{15}N-labeled p53NTD sample were observed upon the addition of Bcl-Xl (Fig. 5), indicating a specific molecular interaction between p53NTD and Bcl-Xl. But owing to the lack of the chemical shift assignments on p53NTD, the

identification of Bcl-Xl-binding site on the p53NTD remains to be defined. The molecular interaction of the N-terminal domain of tumor suppressor p53 with Bcl-Xl appears to be important in the function of p53. While the biological significance of the newly discovered molecular interaction remains to be further studied, our data presented here would provide additional information on transcription-independent mechanism of p53-mediated apoptotic regulation in connection with Bcl-Xl.

Acknowledgments

We thank Dr. Hoi Yeung Li for his valuable advice on FRET assays. This work was generously supported by Ministry of Education of Singapore Grant ARC 4/04.

References

[1] K.H. Vousden, X. Lu, Live or let die: the cell's response to p53, Nat. Rev. Cancer 2 (2002) 594–604.

[2] M. Hollstein, K. Rice, M.S. Greenblatt, T. Soussi, R. Fuchs, T. Sorlie, E. Hovig, B. Smith-Sorensen, R. Montesano, C.C. Harris, Database of p53 gene somatic mutations in human tumors and cell lines, Nucleic Acids Res. 22 (1994) 3551–3555.

[3] B. Vogelstein, D. Lane, A.J. Levine, Surfing the p53 network, Nature 408 (2000) 307–310.

[4] L.J. Hofseth, S.P. Hussain, C.C. Harris, p53: 25 years after its discovery, Trends Pharmacol. Sci. 25 (2004) 177–181.

[5] K. Polyak, Y. Xia, J.L. Zweier, K.W. Kinzler, B. Vogelstein, A model for p53-induced apoptosis, Nature 389 (1997) 300–305.

[6] C. Caelles, A. Helmberg, M. Karin, p53-dependent apoptosis in the absence of transcriptional activation of p53-target genes, Nature 370 (1994) 220–223.

[7] A.J. Wagner, J.M. Kokontis, N. Hay, Myc-mediated apoptosis requires wild-type p53 in a manner independent of cell cycle arrest and the ability of p53 to induce p21waf1/cip1, Genes Dev. 8 (1994) 2817–2830.

[8] Y. Haupt, S. Rowan, E. Shaulian, K.H. Vousden, M. Oren, Induction of apoptosis in HeLa cells by transcription-deficient p53, Genes Dev. 9 (1995) 2170–2183.

[9] X. Chen, L.J. Ko, L. Jayaraman, C. Prives, p53 levels, functional domains, and DNA damage determine the extent of the apoptotic response of tumor cells, Genes Dev. 10 (1996) 2438–2451.

[10] H.F. Ding, Y.L. Lin, G. McGill, P. Juo, H. Zhu, J. Blenis, J.Y. Yuan, D.E. Fisher,

Essential role for caspase-8 in transcription-independent apoptosis triggered by p53, J. Biol. Chem. 275 (2000) 38905–38911.

[11] M.C. Schuler, D.R. Green, Mechanisms of p53-dependent apoptosis, Biochem. Soc. Trans. 29 (2001) 684–688.

[12] N.D. Marchenko, A. Zaika, U.M. Moll, Death signal-induced localization of p53 to mitochondria, J. Biol. Chem. 275 (2000) 16202–16212.

[13] C. Sansome, A. Zaika, N.D. Marchenko, U.M. Moll, Hypoxia death stimulus induces translocation of p53 to mitochondria, FEBS Lett. 488 (2001) 110–115.

[14] P. Dumont, J.I. Leu, A.C. Della Pietra, D.L. George, M. Murphy, The codon 72 polymorphic variants of p53 have markedly different apoptotic potential, Nat. Genet. 33 (2003) 357–365.

[15] S. Cory, J.M. Adams, The Bcl-2 family: regulators of the cellular life-or-death switch, Nat. Rev. 2 (2002) 647–656.

[16] M. Mihara, S. Erster, A. Zaika, O. Petrenko, T. Chittenden, P. Pancoska, U.M. Moll, p53 has a direct apoptogenic role at the mitochondria, Mol. Cell 11 (2003) 577–590.

[17] A.M. Petros, A. Gunasekera, N. Xu, E.T. Olejniczak, S.W. Fesik, Defining the p53 DNA-binding domain/Bcl-Xl-binding interface using NMR, FEBS Lett. 559 (2004) 171–174.

[18] J.E. Chipuk, U. Maurer, D.R. Green, M. Schuler, Pharmacologic activation of p53 elicits Bax-dependent apoptosis in the absence of transcription, Cancer Cell 4 (2003) 371–381.

[19] S. Fields, S.K. Jang, Presence of a potent transcription activating sequence in the p53 protein, Science 249 (1990) 1046–1051.

[20] D. Sakamuro, P. Sabbatini, E. White, G.C. Prendergast, The polyproline region of

p53 is required to activate apoptosis but not growth arrest, Oncogene 15 (1997) 887–898.

[21] J. Chen, V. Marechal, A.J. Levine, Mapping of the p53 and mdm-2 interaction domains, Mol. Cell. Biol. 13 (1993) 4107–4114.

[22] S.M. Picksley, B. Vojtesek, A. Sparks, D.P. Lane, Immunochemical analysis of the interaction of p53 with MDM2—fine mapping of the MDM2 binding site on p53 using synthetic peptides, Oncogene 9 (1994) 2523–2529.

[23] S. Bell, C. Klein, L. Müller, S. Hansen, J. Buchner, p53 contains large unstructured regions in its native state, J. Mol. Biol. 322 (2002) 917– 927.

[24] R. Dawson, L. Müller, A. Dehner, C. Klein, H. Kessler, J. Buchner, The N-terminal domain of p53 is natively unfolded, J. Mol. Biol. 332 (2003) 1131–1141.

[25] C.B. Kang, L. Feng, J. Chia, H.S. Yoon, Molecular characterization of FK-506 binding protein 38 and its potential regulatory role on the anti-apoptotic protein Bcl-2, Biochem. Biophys. Res. Commun. 337 (2005) 30–38.

[26] B.A. Johnson, R.A. Blevins, NMRView: A computer program for the visualization and analysis of NMR data, J. Biomol. NMR 4 (1994) 603–614.

[27] C.B. Kang, J. Tai, J. Chia, H.S. Yoon, The flexible loop of Bcl-2 is required for molecular interaction with immunosuppressant FK506 binding protein 38 (FKBP38), FEBS Lett. 579 (2005) 1469–1476.

[28] A.K. Kenworthy, Imaging protein–protein interactions using fluorescence resonance energy transfer microscopy, Methods 24 (2001) 289–296.

[29] T.S. Karpova, C.T. Baumann, L. He, X. Wu, A. Grammer, P. Lipsky, G.L. Hager, J.G. McNally, Fluorescence resonance energy transfer from cyan to yellow fluorescent protein detected by acceptor photobleaching using confocal microscopy

and a single laser, J. Microsc. 209 (2003) 56–70.

[30] A.M. Bode, Z. Dong, Post-translational modification of p53 in tumorigenesis, Nat. Rev. Cancer 4 (10) (2004) 793–805.

[31] K.K. Walker, A.J. Levine, Identification of a novel p53 functional domain that is necessary for efficient growth suppression, Proc. Natl. Acad. Sci. USA 93 (1996) 15335–15340.

List of Figures

addition of p53NTD is presented in blue. Concentration of ^{15}N-labeled Bcl-Xl was 0.5 mM. Concentrations of ^{15}N-labeled Bcl-Xl and p53NTD were 0.5 and 0.25 mM, respectively. (B) Section of a ^{15}N HSQC NMR titration spectrum. Amino acid L112 and E129 chemical shifts were changed upon the addition of increasing amount of p53NTD from 0 to 0.75 mM as displayed. V86, K87, L99, E129, L178, and T190 do not show chemical shift changes. (For interpretation of the references to colour in this figure legend, the reader is referred to the web version of this paper.)

Fig. 4 Mapping of p53NTD-Bcl-Xl interaction on Bcl-Xl. (A) Ribbon representation of Bcl-Xl. Amino acids perturbed upon the addition of p53NTD are shown in green. (B) Ribbon representation of Bcl-Xl (PDB1BXL). BH1, BH2, and BH3 regions are shown in pink. (For interpretation of the references to colour in this figure legend, the reader is referred to the web version of this paper.)

Fig. 5 2D ^{1}H–^{15}N HSQC spectrum recorded on ^{15}N-labeled p53NTD in the absence (in red) and presence (in black) of unlabeled Bcl-Xl. Concentrations of ^{15}N-labeled p53NTD and Bcl-Xl were 0.25 and 0.375 mM, respectively. (For interpretation of the references to colour in this figure legend, the reader is referred to the web version of this paper.)

Fig. 6 Molecular interaction between p53 NTD and Bcl-Xl in a FRET assay. (A) FRET was used to illustrate the existence of the binding between p53NTD and

Bcl-Xl. NCI-H1299 cells co-expressing p53NTD-YFP and Bcl-Xl-CFP were cultured at 37 °C for 16–18 h before FRET assay. Images of NCI-H1299 cells in CFP and YFP channels before and after acceptor photobleaching are shown. The bleached region was outlined by black dashed square box, whereas white dashed box indicates the unbleached (control) region. (B) Histogram shows quantification of FRET. The increase in CFP fluorescence intensity in bleached (black columns) and control unbleached (white columns) cells. The data represent the average of three experiments.

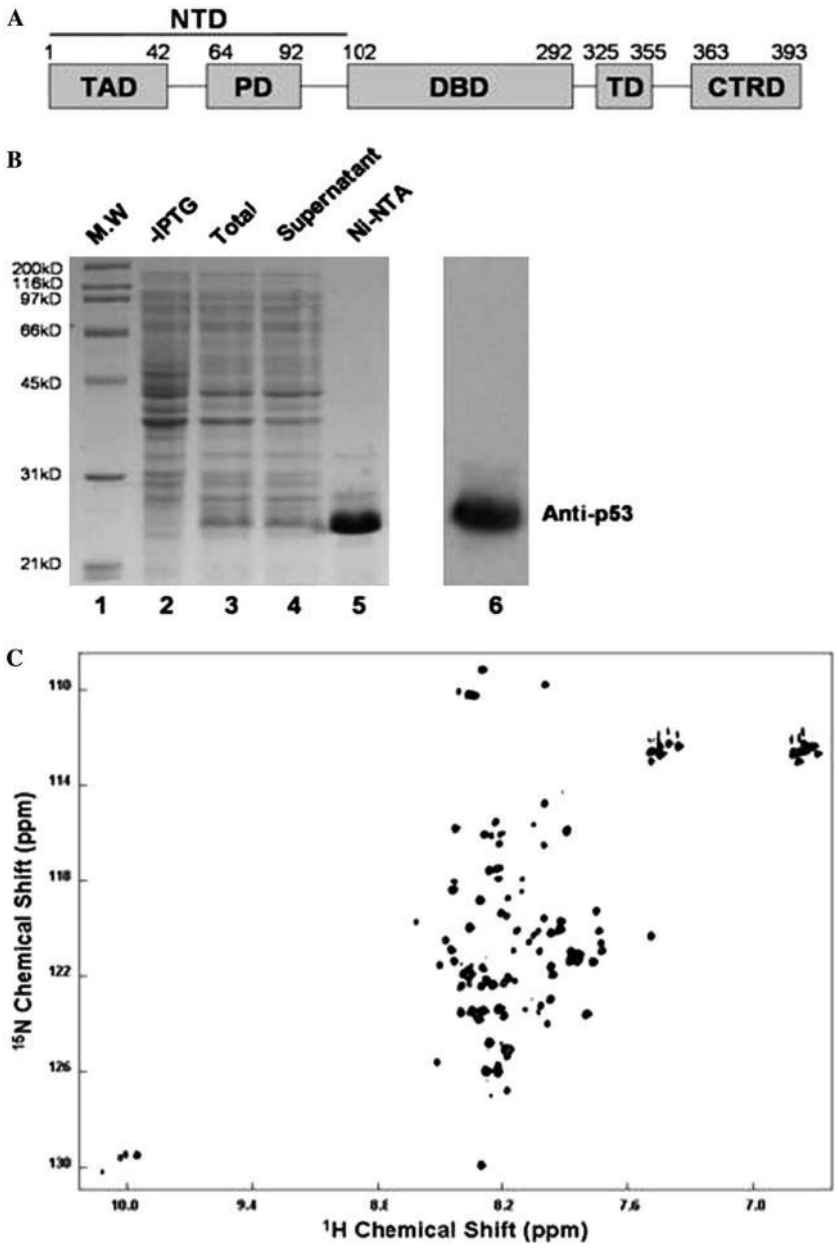
A
NTD
1
42
64
92
102
292
325
355
363
393
TAD
PD
DBD
TD
CTRD
B
M.W
-IPTG
Total
Supernatant
Ni-NTA
200kD
116kD
97kD
66kD
45kD
31kD
21kD
Anti-p53
1
2
3
4
5
6
C
110
114
118
122
126
130
15N Chemical Shift (ppm)
10.0
9.4
8.8
8.2
7.6
7.0
1H Chemical Shift (ppm)

Fig.1

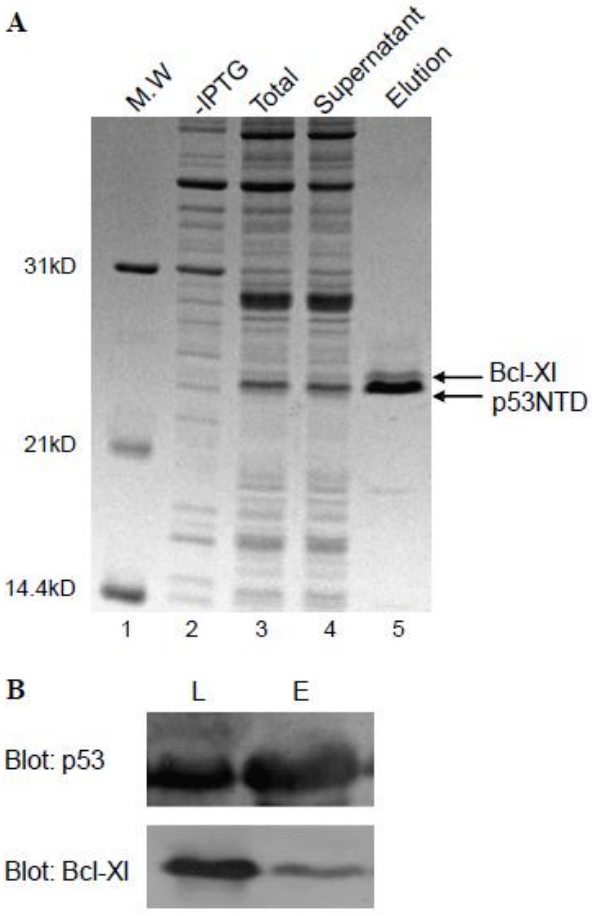
A
M.W
-IPTG
Total
Supernatant
Elution
31kD
21kD
14.4kD
Bcl-XI
p53NTD
1
2
3
4
5
B
L
E
Blot: p53
Blot: Bcl-XI

Fig. 2

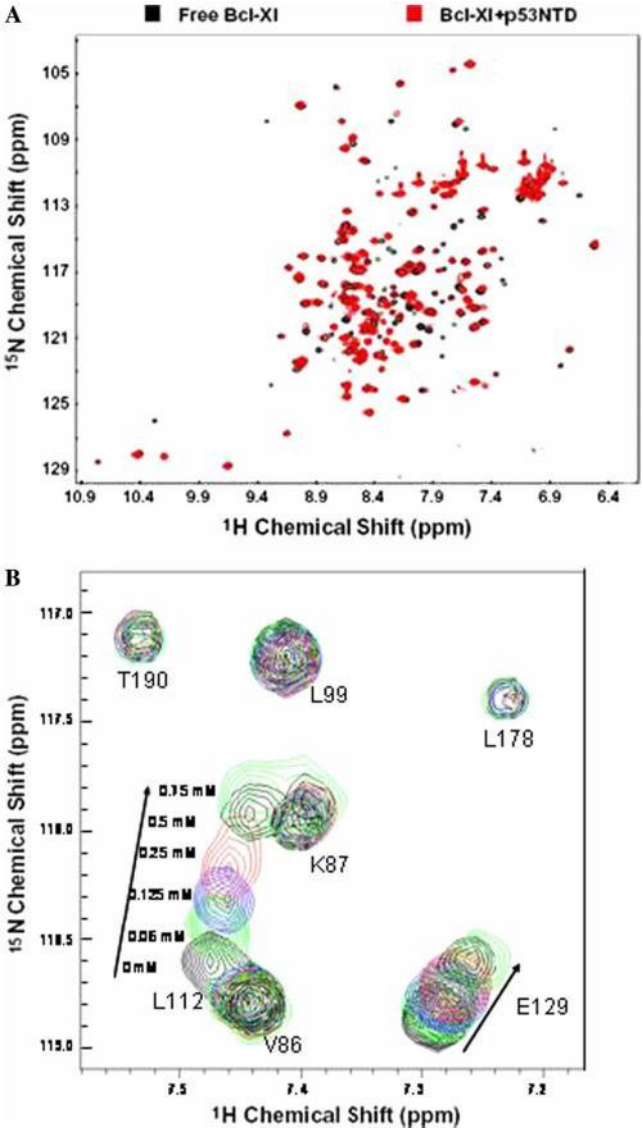
A
Free Bcl-XI
Bcl-XI+p53NTD
15N Chemical Shift (ppm)
1H Chemical Shift (ppm)
B
T190
L99
L178
K87
L112
V86
E129
0.35 mM
0.5 mM
0.25 mM
0.125 mM
0.06 mM
0 mM
15N Chemical Shift (ppm)
1H Chemical Shift (ppm)

Fig. 3

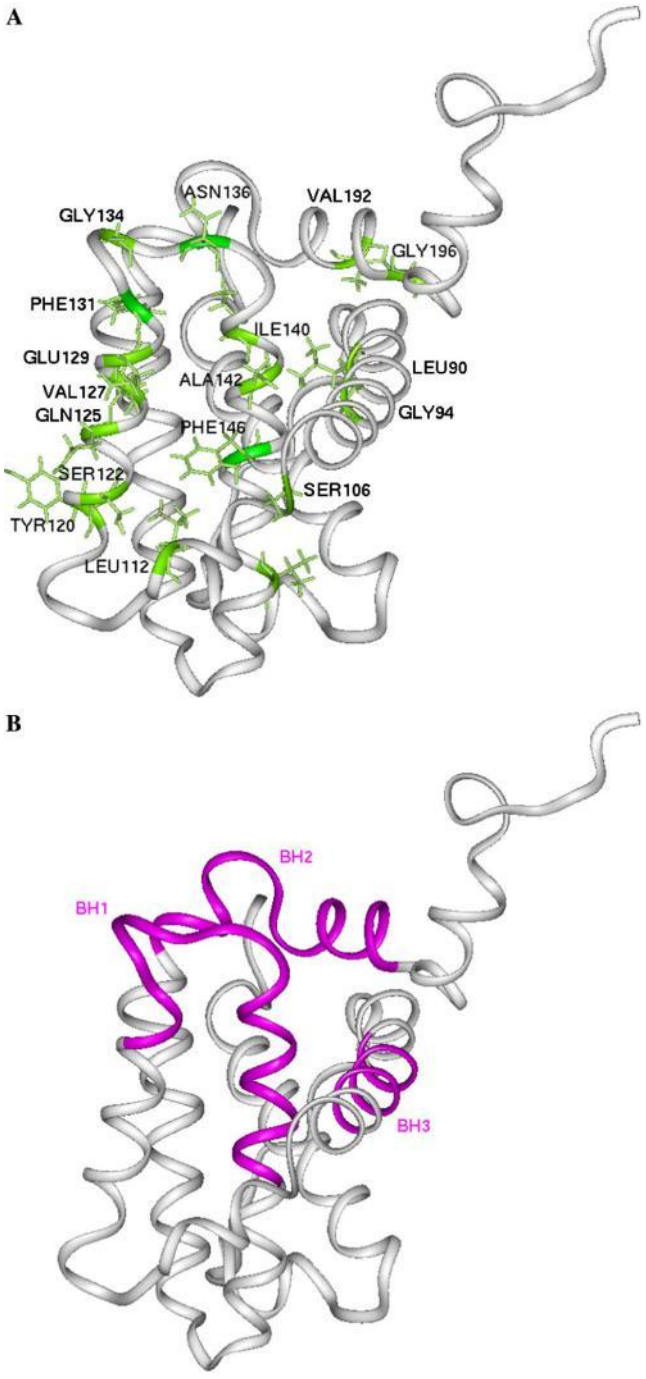
A
ASN136
VAL192
GLY134
GLY196
PHE131
ILE140
GLU129
LEU90
ALA142
VAL127
GLN125
GLY94
PHE146
SER122
SER106
TYR120
LEU112
B
BH2
BH1
BH3

Fig. 4

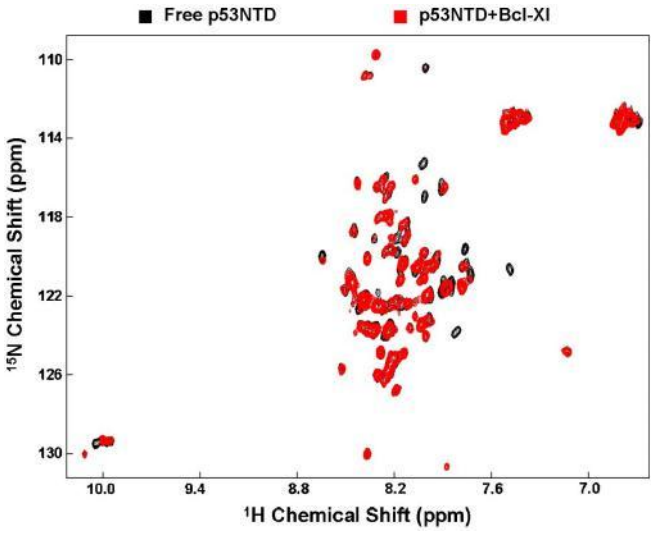
Free p53NTD
p53NTD+Bcl-Xl
110
114
118
122
126
130
15N Chemical Shift (ppm)
10.0
9.4
8.8
8.2
7.6
7.0
1H Chemical Shift (ppm)

Fig.5

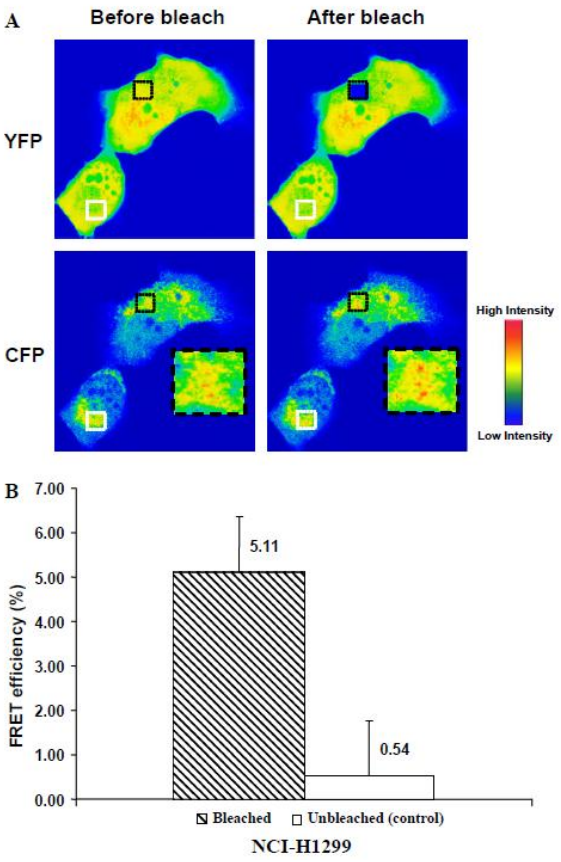
A
Before bleach
After bleach
YFP
CFP
High Intensity
Low Intensity
B
FRET efficiency (%)
7.00
6.00
5.00
4.00
3.00
2.00
1.00
0.00
5.11
0.54
Bleached
Unbleached (control)
NCI-H1299

Fig. 6